Three-dimensional visualization of natural convection of miscible fluids due to the density difference in a packed bed

T. Suekane & S. Sakai
Department of Energy Sciences, Tokyo Institute of Technology, Japan

Abstract

Understanding of natural convection of miscible two phases in porous media is of great importance to problems of geological storage of carbon dioxide. We consider saltwater–freshwater fingering instabilities in a saturated porous medium. Plastic resin particles with an average diameter of 320 μm or 440 μm were packed 50 mm in height in a tube with the inter diameter of 32 mm. Development of the fingering due to instabilities and natural convection of freshwater and saltwater in porous media have been imaged by means of micro-focused X-ray computer tomography (CT) every three minutes. At early stages of convective mixing, ripples appear on the contour surface of the concentration of sodium iodine and grow to be fingers which extend vertically downwards with time. As fingers proceed downwards, the concentration of sodium iodine in fingers are reduced. As a result the convective mixing is rapidly suppressed. With an increase in the density difference and the permeability, the development of the natural convection occurs more quickly. The standard deviation of CT values in the particle pack was used to evaluate the critical time and the mixing time of natural convection. The estimated critical time is in the range between 200 s and 600 s. The mixing time estimated in present work agrees well with the linear stability analysis. Convective mixing processes are modeled with a one-dimensional diffusion equation with an apparent diffusion coefficient, of which order is in the range from 10^{-6} to 10^{-5} m^2/s.
Keywords: natural convection, X-ray imaging, fingering, Rayleigh–Darcy number.


WIT Transactions on Engineering Sciences, Vol 89, © 2015 WIT Press
www.witpress.com, ISSN 1743-3533 (on-line)
doi:10.2495/MPF150401

1 Introduction

Carbon dioxide (CO_2) is the most important anthropogenic greenhouse gas. The global atmospheric concentration of CO_2 has increased from a pre-industrial value of approximately 280 ppm to 379 ppm in 2005. The warming of the climate system is unequivocal, as is now evident from observations of increasing global average air and ocean temperatures, widespread melting of snow and ice and rising global average sea level [1]. To stabilize the concentration of CO_2 in the atmosphere, emissions need to peak and then decline thereafter. For lower stabilization targets, scenarios put more emphasis on the use of low-carbon energy sources, such as renewable energy and nuclear power, and the use of CO_2 capture and storage (CCS) [2, 3].

The safety of geologic storage of CO_2 is obviously a central concern in planning carbon sequestration on a large scale. The current concept of geologic storage involves the injection of CO_2 into deep formations, which typically contain brine. CO_2 is supercritical at temperatures and pressures above the critical values of 304 K and 7.38 MPa. In typical geologic formations, the critical condition of CO_2 is reached at a depth of approximately 740 m. Because of geologic pressure, the density of CO_2 dramatically increases with depth; however, the density of CO_2 is approximately 0.9 times that of water, so when CO_2 is injected into the subsurface, buoyancy tends to bring CO_2 upward in geologic formations. On the other hand, CO_2 will be retained by physical and geochemical mechanisms, such as physical trapping [4], capillary trapping [5–11], solubility trapping [12–17] and mineralization [18].

Weir *et al.* [19] pointed out that all of the gas injected into deep reservoirs dissolves into the water, and the resulting dense fluid settles in the aquifer over several thousand years in the most favourable case. Lindeberg and Wessel-Berg [12] analytically discussed the stability criteria for convectional vertical flow. Ennis-King *et al.* [20] studied to estimate the time required for the instability to occur using linear stability analysis. Reservoir simulations provide an insight into the development of convective mixing due to density difference [21–26] including for heterogeneous aquifers [27–29]. Macminn *et al.* [30] developed semi-analytical models to study the competition between capillary and solubility trapping.

Most of these works used numerical simulation techniques and/or analytical models, but there are few experimental studies which verify these works. Recent development on X-ray CT scanning or magnetic resonance imaging [31] allows us to three-dimensionally visualize the convective mixing in a porous medium.

This paper describes experimental research on natural convection due to the density difference between the sodium iodine solution and pure water in porous media. The development of fingers and the convective mixing processes were visualized by using an X-ray CT scanner. We discuss the development of natural convection and effect of density difference and permeability to them. Next, the critical time and the mixing time are evaluated from the experimental results and are compared with the analytical results. Finally, the convective mixing

processes are modelled with a one-dimensional diffusion equation with an apparent diffusion coefficient.

2 Experimental procedure and analytical parameters

2.1 Experimental setup and procedure

We used packed beds of melamine resin particles as a porous medium as shown in Fig. 1. Particles were packed in the 50 mm high pipe with inner diameter of 32 mm. We used two kinds of particle; one diameter in the range between 230 μm and 410 μm with an average diameter of 320 μm (Ube Sand Engineering Co. Ltd., XH40/60), and the other has a diameter in the range between 380 μm and 580 μm with an average diameter of 480 μm (XH30/40).

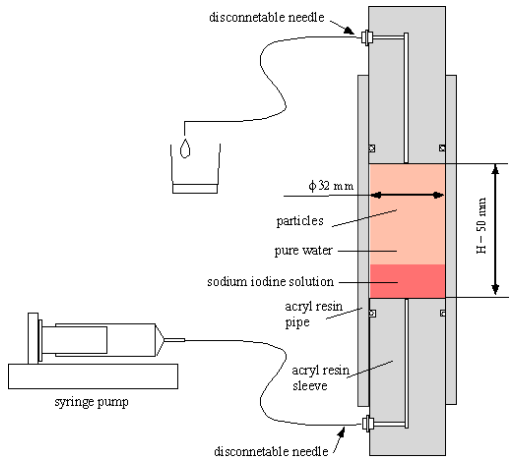

Figure 1: Experimental apparatus.

Pure water and water doped with sodium iodine with four concentrations were used as miscible fluids. Sodium iodine solutions are feasible to evaluate concentration from CT images, because of high attenuation coefficient of sodium iodine against X-ray as mentioned later. Experimental conditions are summarized in Table 1. The absolute permeability of particle packs is estimated with the Kozeney–Carman equation

$$k = \frac{d_m^2}{180} \frac{\phi^3}{(1-\phi)^2} \tag{1}$$

All experiments were performed at a room temperature of 25°C. First, a particle pack was filled with distilled water by using a vacuum chamber. The difference in weight between before and after water filling shows that the porosity of the particle packs is 0.365. Second, sodium iodine solution was injected into the vertically aligned particle pack from the bottom to avoid instability of displacing interface. When quarter of the pack was filled with

sodium iodine solution, injection was stopped and tubes to inject and drain fluids were carefully disconnected. The pack is put in an X-ray CT scanner (Comscantechno Co. Ltd., ScanXmate-G100S110) for measurements of concentration of sodium iodine in solution prior to the natural convection experiments. The ratio of height of sodium iodine to that of the particle pack was 0.18 on average.

Table 1: Experimental conditions.

Run #	Average beads diameter, d_m, μm	Absolute permeability, $k \times 10^{10}$, m^2	Initial concentration of sodium iodine C_0, wt %	Density Ratio	Rayleigh Darcy number, $Ra \times 10^4$
Run 1-1	320 (230–410)	0.686	7.5	1.07	0.776
Run 2-1			15	1.14	1.55
Run 3-1			30	1.29	3.10
Run 4-1			40	1.41	4.14
Run 1-2	480 (380–580)	1.54	7.5	1.07	1.74
Run 2-2			15	1.14	3.48
Run 3-2			30	1.29	6.97
Run 4-2			40	1.41	9.29

Immediately after the particle pack is turned upside down, natural convection due to the density difference is caused in the pack. The pack was scanned every 3.0 minutes, because it took approximately two minutes to perform a single scan. The time at the beginning of the scan is assigned as time of the scan. The scan was continued for 45 minutes.

The X-ray scanner is set at a 119 μA current and 74 kV voltage with a flame rate of 6 flame/sec. Reconstructed three-dimensional images which covers a whole domain of the particle pack consist of 608 × 608 × 495 pixels at a resolution of 167.0 μm/pixel. Each pixel has a CT value proportional to the concentration of sodium iodine in water. The CT values scanned prior to start natural convection provide two sets of known concentration for calibration.

2.2 Analytical parameters

The Rayleigh–Darcy number:

$$Ra = \frac{g\rho_0\beta_c kHC_0}{\mu_w \phi D} \tag{2}$$

is a dimensionless parameter which governs the density-driven natural convection in porous media [32].

The critical time at which instability occurs should scale as:

$$t_c = c_1 D\left(\frac{\mu_w \phi}{\Delta\rho g k}\right)^2 \tag{3}$$

where $\Delta\rho = \rho_0\beta_c C_0$ and c_1 is a dimensionless constant [20, 30, 32]. The critical wavelength λ_c is estimated as:

$$t_{mix} = \frac{H\mu_w}{\Delta\rho g k} \tag{4}$$

where the constant parameter $c_2 = 96.23$ [32].

The time required to mix in the particle pack can be estimated as:

$$t_{mix} = \frac{H\mu_w}{\Delta\rho g k} \tag{5}$$

because a characteristic convective (Darcy) velocity is expressed as $\Delta\rho g k/\mu_w$ [33].

3 Experimental results and discussion

3.1 Characteristics of convective mixing

Development of natural convection in the particle pack is shown in Fig. 2 for the Run 1-1. Top and bottom sides and left and right sides of images are sleeves and a tube of a packed bed. Because the image resolution of 167.0 μm/pixel is approximately half of the mean particle diameter of 320 μm, the brightness of each pixel represents an X-ray attenuation coefficient averaged over the domain which contains a few pores and particles. The brightness for various sodium iodine concentrations shown in Table 1 shows that it is proportional to the concentration for both particle packs.

At 270 s a finger develops along the region on the wall with high permeability because of sorting of particles. Several fingers appear on the interface at 450 s and grow with time. The fingers have a diameter of approximately 3–5 mm, which is an order of magnitude larger than the particle diameter. The finger diameter is 5–9 times larger than the critical wavelength of 6.20×10^{-4} m estimated by Equation (4). After 990 s, the mixing of two fluids slows down rapidly. The concentration of sodium iodine in fingers is reduced by mixing with pure water which previously occupies the pores. At $t = 2790$ s, the interface of fingers blurred.

Fig. 3 shows the contour surfaces of sodium iodine concentration for the Run 1-1 and Run 2-1 at early stages of convective mixing. The contour surfaces were already rippled at $t = 90$ s (Figs. 3(a) and 3(d)). This perturbation on the interface was caused during the injection process of sodium iodine solution into a water filled particle pack. As time progresses, ripples due to the density difference instability appear on the contour surfaces and grow downwards. The development of the fingers is faster for higher density ratio. The linear stability analysis shows the critical wavelength is inversely proportional to the density difference as Equation (4), but the fingers of Run 1-1 and Run 2-1 have same diameters.

3.2 Critical time and mixing time

For the sake of evaluation of the critical time and mixing time based on X-ray CT images, we estimated the standard deviation of CT value within the particle pack as shown in Fig. 4. The standard deviation is normalized with these before

a turnover of the particle pack and at t = 2,790 s for each experimental run. The mixing becomes faster with increasing density ratio and with increasing permeability.

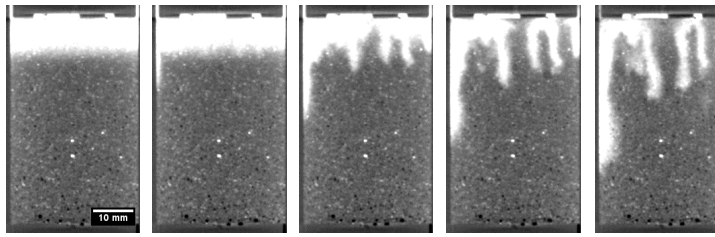

(a) 90 s (b) 270 s (c) 450 s (d) 630 s (e) 810 s

(f) 990 s (g) 1170 s (h) 1350 s (i) 1530 s (j) 2790 s

Figure 2: Vertical cross-sectional X-ray CT images for the Run 1-1. Brightness is proportional to the concentration of sodium iodine. (a) The region where top 18 % of the particle pack in height is filled with the sodium iodine solution at the concentration of 7.5 w% and the rest region were filled with pure water. Images (a)–(i) were scanned every three minutes, but the interval between (i) and (j) is 21 minutes.

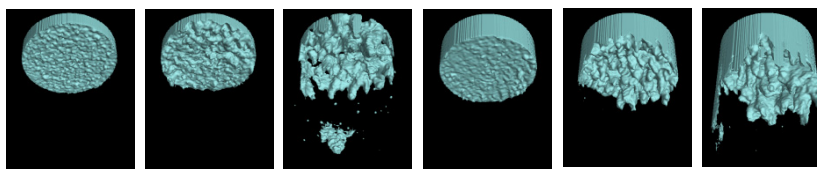

(a) Run 1-1, t = 90 s (b) 270 s (c) 450s (d) Run 2-1, 90 s (e) 270 s (f) 450 s

Figure 3: A view from below shows the development of fingers on the boundary for Run 1-1 ((a)–(c)) and Run 2-1 ((d)–(f)). The surface corresponds to a concentration of an approximately half value of initial concentration.

The critical time and the mixing time were evaluated as follows. Three points centered with the inflection point were fitted with a straight line. The critical time was evaluated from the distance from the point t = 0 to the point of intersection of the regression line and $\overline{\sigma} = 1$. The mixing time was evaluated by subtracting the critical time from the time when the normalized standard deviation reduces to e^{-1}.

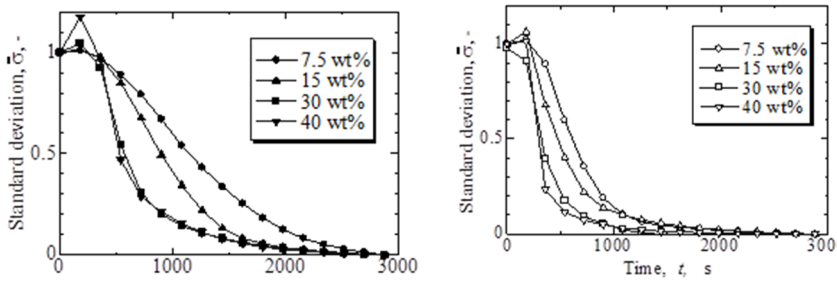

Figure 4: Change in the normalized standard deviation with time for the average particle diameter of (a) d_m = 320 μm and (b) 480μm.

Fig. 5 shows the critical time plotted against the scaling parameter in Equation (3). The estimated critical time is in the range between 200 s and 600 s. Because the interval of the scans was 180 s, the estimated critical time has a large error especially for short cases. The lines represent the critical time estimated by Equation (3) with a dimensionless coefficient of c_1 = 10,000 and 100,000. Pau *et al.* [22] found that c_1 = 3,670 by numerical simulations. To evaluate the dimensionless constant from the experimental results, we should reduce the interval of scanning. However, the dimensionless coefficient is estimated as c_1~10^4 – 10^5.

Fig. 6 shows the relation between the mixing time of present experiments and the analytical results expressed by Equation (5). All experimental results agree well with Equation (5). The tendency that the experimental results are longer than Equation (5) is due to the definition of the mixing time to estimate it from Fig. 4.

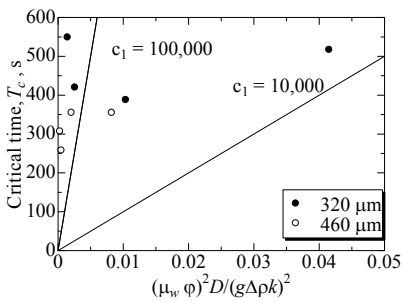

Figure 5: Relation between the critical time obtained from the experiments and the scaling parameter in Equation (3).

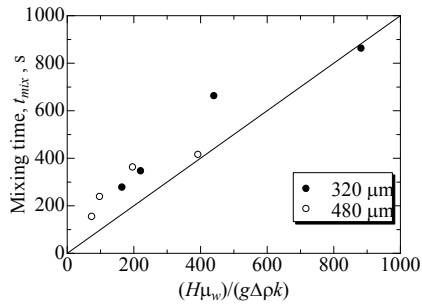

Figure 6: Relation between the mixing time obtained from the experiments and the analytical results expressed in Equation (5).

3.3 Apparent diffusion coefficient

Convective mixing process can be modeled as a one-dimensional unsteady classical diffusion problem with Fick's law. Assuming a constant diffusion coefficient, the homogeneous Neumann problem is formulated as:

$$\frac{\partial C}{\partial t} = D_a \frac{\partial^2 C}{\partial z^2} \tag{6}$$

where D_a denotes the apparent diffusion coefficient. The boundary and initial conditions are:

$$\frac{\partial C}{\partial z}(0,t) = \frac{\partial C}{\partial z}(H,t) = 0, \quad t > 0\,; \tag{7}$$

$$C(z,0) = f(z), \quad 0 < z < H\,, \tag{8}$$

respectively. The solution of Equation (1) with these boundary and initial conditions are:

$$C(z,t) = \sum_{n=0}^{\infty} A_n \cos\left(\frac{n\pi z}{H}\right) \cdot \exp\left(-\left(\frac{n\pi}{L}\right) D_a t\right) \tag{9}$$

and the A_n are the Fourier cosine series coefficients of $f(z)$, so that

$$A_n = \frac{2}{H} \int_0^H f(z) \cos\left(\frac{n\pi z}{H}\right) dz, \quad n \geq 1\,; \tag{10}$$

and for $n = 0$,

$$A_0 = \frac{1}{H} \int_0^H f(z) dz. \tag{11}$$

Comparing the deviation of the solution 6 with that of experimental results, we can evaluate the apparent diffusion coefficient. Because the analytical derivation of the deviation is a complicated problem, we solved numerically the diffusion Equation (6) with the initial conditions:

$$f(z) = C_0, \quad 0 < z < 0.18H\,, \tag{12}$$

$$f(z) = 0, \quad 0.18H < z < H\,, \tag{13}$$

where C_0 is the initial concentration of sodium iodine, the value of which is independent of the normalized deviation of a solution.

Fig. 7 shows the standard deviation of the concentration plotted against $(D_a t)^{1/2}$. Numerical simulation results for various apparent diffusion coefficients fall on the same line. The fraction of height of sodium iodine to that of the particle pack affects the profile of the standard deviation. The linear approximation for the profile at early stages $0 < (D_a t)^{1/2} < 0.01$ gives the correlation equation. If the standard deviation of experimental results shown in Fig. 4 is plotted against $t^{1/2}$, the gradient equals $54.58 \cdot D_a^{1/2}$. We evaluated the apparent diffusion coefficient as this manner.

Fig. 8 shows the obtained apparent diffusion coefficient plotted against Rayleigh–Darcy number. The order of the effective diffusion coefficient is in the range from 10^{-6} to 10^{-5} m^2/s, which is three or four orders of magnitude larger than the molecular diffusion coefficient. The apparent diffusion coefficient increases with the Rayleigh–Darcy number for each particle diameter.

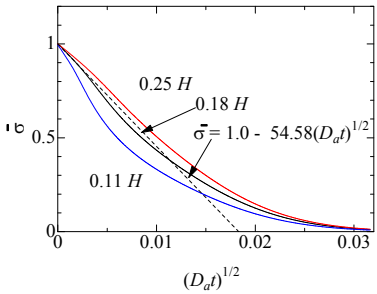

Figure 7: Normalized standard deviation of the sodium iodine concentration scaled with $(D_at)^{1/2}$.

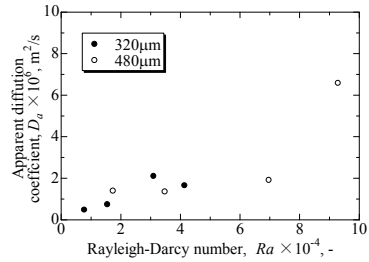

Figure 8: Effective diffusion coefficient.

4 Conclusions

This paper describes experimental research on natural convection due to the density difference between the sodium iodine solution and pure water in porous media. The development of fingers and the convective mixing processes were visualized by using an X-ray CT scanner.

At early stages of convective mixing, ripples appear on the contour surface of the concentration of sodium iodine and grow to be fingers which extend vertically downwards with time. At the condition of the initial concentration of sodium iodine of 7.5 wt% and the particle diameter of 320 μm, the fingers have a diameter of approximately 3–5 mm, which is 5–9 times larger than the critical wavelength estimated by the linear stability analysis. As fingers proceed downwards, the concentration of sodium iodine in fingers are reduced. As a result the convective mixing is rapidly suppressed. With an increase in the density difference and the permeability, the development of the natural convection occurs more quickly.

The standard deviation of CT values in the particle pack was used to evaluate the critical time and the mixing time of natural convection. The estimated critical time is in the range between 200 s and 600 s, which contains a large error, because the scanning interval is 180 s. However, the dimensionless coefficient is estimated as $c_1 \sim 10^4 - 10^5$. The mixing time estimated in present work agrees well with the linear stability analysis.

Convective mixing processes are modeled with a one-dimensional diffusion equation with an apparent diffusion coefficient. The apparent diffusion coefficient increases with the Rayleigh–Darcy number for each particle diameter. The order of the effective diffusion coefficient is in the range from 10^{-6} to 10^{-5} m^2/s.

Nomenclature

C	concentration of sodium iodine, kg/m^3
C_0	initial concentration of sodium iodine, kg/m^3
c_1 ,c_2	dimensionless constant
D	molecular diffusion coefficient, m^2/s
D_a	apparent diffusion coefficient, m^2/s
d_m	average particle diameter, m
g	gravitational acceleration, m/s^2
H	height of particle pack, m
k	absolute permeability, m^2
Ra	Rayleigh–Darcy number
t	time, s
t_c	critical time for instability to develop, s
t_{mix}	time for mixing to occur, s
z	vertical coordinate, m
β_c	expansion coefficient, m^3/kg
$\Delta\rho$	density difference, kg/m^3
λ_c	critical wavelength, m
μ_w	viscosity of water, Pa·s
ρ_0	density of pure water, kg/m^3
ϕ	porosity

References

[1] IPCC, Climate Change 2007: The Physical Science Basis. Contribution of working Group I to the Fourth Assessment Report of the Intergovernmental Panel on Climate Change. Solomon, S., Qin, D., Manning, M., Chen, Z., Marquis, M., Averyt, K.B., Tignor, M. & Miller, H.L. (eds.), Cambridge University Press, ISBN 978-0-521-70597-7 New York, USA, 2007.

[2] Pacala, S. & Socolow, R., Stabilization Wedge: Solving the Climate Problem for the Next 50 Years with Current Technologies. Science, pp. 96–972, 305, 2004.

[3] IPCC, Climate Change 2007: Mitigation of Climate Change. Contribution of working Group III to the Fourth Assessment Report of the Intergovernmental Panel on Climate Change. B. Metz; O.R. Davidson; P.R. Bosch; R. Dave & L.A. Meyer (eds.), Cambridge University Press, ISBN 978-0-521-70598-1 New York, USA, 2007.

[4] IPCC, IPCC Special Report on Carbon Dioxide Capture and Storage. Metz, B.; Davidson, O.; de Coninck, H.C.; Loos, M. & Meyer, L.A. (eds.), Cambridge University Press, Cambridge, UK and USA pp. 195–276, 2005.

[5] Suekane, T., Nobuso, T., Hirai, S. & Kiyota, M., Geological Storage of Carbon Dioxide by Residual Gas and Solubility Trapping. International Journal of Greenhouse Gas Control, pp. 58–64, 2, 2008.

[6] Suekane, T., Zhou, N., Hosokawa, T. & Matsumoto, T., Direct Observation of Gas Bubbles Trapped in Sandy Porous Media. Transport in Porous Media, pp. 111–122, 82, 2010.

[7] Al Mansoori, S.K., Itsekiri, E., Iglauer, S., Pentland, C.H., Bijeljic, B. & Blunt, M.J., Measurements of Non-Wetting Phase Trapping Applied to Carbon Dioxide Storage. International Journal of Greenhouse Gas Control, pp. 283–288, 4, 2008.
[8] Pentland C.H., El-Maghraby, R., Georgiadis, A., Iglauer, S. & Blunt, M.J., Immiscible Displacement and Capillary Trapping in CO_2 Storage. Presented at 10th International Conference on Greenhouse Gas Control Technologies, Amsterdam, The Netherlands, September 19–23, 2010.
[9] Zhou, N., Matsumoto, T., Hosokawa, T. & Suekane, T., Pore-Scale Visualization of Gas Trapping in Porous Media by X-ray CT Scanning. Flow Measurement and Instrumentation, pp. 262–267, 21, 2010.
[10] Wildenschild, D.; Armstrong R.T.; Herring, A.L.; Young, I.M. & Carey, J.W. Exploring Capillary Trapping Efficiency as a Function of Interfacial Tension, Viscosity, and Flow Rate. Presented at 10th International Conference on Greenhouse Gas Control Technologies, Amsterdam, The Netherlands, September 19–23, 2010.
[11] Saadatpoor, E., Bryant, S.L. & Sepehrnoori, K., Effect of Upscaling Heterogeneous Domain on CO_2 Trapping Mechanisms. Presented at 10th International Conference on Greenhouse Gas Control Technologies, Amsterdam, The Netherlands, September 19–23, 2010.
[12] Lindeberg, E. & Wessel-Berg, D., Vertical Convection in an Aquifer Column under a Gas Cap of CO_2, Energy Convers. Mgmt, Suppl., S229–S234, 38, 1997.
[13] McPherson, B.J.O.J. & Cole, B.S., Multiphase CO_2 Flow, Transport and Sequestration in the Powder River Basin, Wyoming, USA. Journal of Geochemical Exploration, pp. 65–70, 2000.
[14] Ennis-King, J., Gibson-Poole, C.M., Lang, S.C. & Paterson, L., Long Term Numerical Simulation of Geological Storage of CO_2 in the Petral Sub-Basin, North West Australia, Proceeding of 6th International Conference on Greenhouse Gas Control Technologies, J. Gale & Y. Kaya (eds.) Vol. 1, Kyoto, Japan, October 1–4, 2002.
[15] Gilfillan, S.M.V., Lollar, B.S., Holland, G., Blagburn, D., Stevens, S., Schoell, M., Cassidy, M., Ding, Z., Zhou, Z., Lacrampre-Couloume, G. & Ballentine, C.J., Solubility Trapping in Formation Water as Dominant CO_2 Sink in Natural Gas Fields, Nature, pp. 614–618, 458, 2009.
[16] Iding, M. & Blunt, M.J., Enhanced Solubility Trapping of CO_2 in Fractured Reservoirs, Presented at 10th International Conference on Greenhouse Gas Control Technologies, Amsterdam, The Netherlands, September 19–23, 2010.
[17] Iglauer, S., Dissolution Trapping of Carbon Dioxide in Reservoir Formation Brine – A Carbon Storage Mechanism, In: Mass Transfer – Advanced Aspect, Nakajima, H, (ed.) pp. 233–262, 2011.
[18] Gunter, W.D. Perkins, E.H. & McCann, T.J. Aquifer Disposal of CO_2-Rich Gases: Reaction Design for Added Capacity. Energy Conversion and Management. pp. 941–748, 34, 1993.
[19] Weir, G.J., White, S.P. & Kissling, W.M., Reservoir storage and containment of greenhouse gases, II: Vapour-entry pressures. Transp

Porous Med, pp. 36–60, 23, 1996.
[20] Ennis-King, J., Bradshaw, J., Gibson-Poole, C., Hennig, A., Lang, S., Paterson, L., Root, R., Sayers, J., Spencer, L., Streit, J. & Undershultz, J, Long-term numerical simulation of a portfolio of possible sites for geological storage of carbon dioxide in Australia, Proceedings of the 7th International Conference on Greenhouse Gas Control Technologies, 2005.
[21] Lindeberg, E. & Bergmo, P, The Long-Term Fate of CO_2 Injected into an Aquifer, In: Greenhouse Gas Control Technologies, Gale, J, Kaya, Y (eds.) Elsevier Science Ltd. Proceedings of the 6th International Conference on Greenhouse Gas Control Technologies, Kyoto Japan, 2003.
[22] Pau, G.S.H., Bell, J.B., Pruss, K., Almgren, A.S., Lijewski, M.J. & Zhang, K., High-resolution Simulation and Characterization of Density-Driven Flow in CO_2 Storage in Saline Aquifers, Adv. Water Res, pp. 443–455, 33, 2010.
[23] Law, D.H.-S. & Bachu, S., Hydrogeological and Numerical Analysis of CO_2 Disposal in Deep Aquifers in the Alberta Sedimentary Basin, Energy Convers. Mgmt, pp. 1167–1174, 37, 1996.
[24] Hassanzadeh, H., Pooladi-Darvish, M. & Keith, D.W., Modeling of Convective Mixing in CO_2 Storage. Journal of Canadian Petroleum Technology, pp. 42–52, 44, 2005.
[25] Ennis-King, J. & Paterson, L., Role of Convective Mixing in the Long-Term Storage of Carbon Dioxide in Deep Saline Formations, SPE J. pp. 349–356, 2005.
[26] Javaheri, M., Abedi, J., Hassanzadeh, H., Linear Stability Analysis of Double-Diffusive Convection in Porous Media, with Application to Geological Storage of CO_2, Transp Porous Med, pp. 441–456, 84, 2010.
[27] Lindeberg, E. & Wessel-Berg, D., Upscaling Studies of Diffusion Induced Convection in Homogeneous and Heterogeneous Aquifers, Energy Procedia, pp. 3927–3934, 4, 2011.
[28] Chen, C. & Zhang, D., Pore-scale Simulation of Density-Driven Convection in Fractured Porous Media During Geological CO_2 Sequestration, Water Resour. Res, W11527, 46, 2010.
[29] Pruss, K. & Nordbotten, J., Numerical Simulation Studies of the Long-term Evolution of a CO_2 Plume in a Saline Aquifer with a Sloping Caprock, Transp Porous Med, pp. 135–151, 90, 2011.
[30] Macminn, C.W., Szulczewski, M.L. & Juanes, R., CO_2 Migration in Saline Aquifers. Part 2. Capillary and Solubility Trapping, J. Fluid Mech., pp. 321–351, 688, 2011.
[31] Johannsen, K., Oswald, S., Held, R. & Kinzelback, W., Numerical Simulation of Three-dimensional Saltwater-freshwater Fingering instabilities observed in a porous medium, Adv. Water Resources, pp. 1690–1704, 29, 2006.
[32] Xu, X., Chen, S. & Zhang, D., Convective Stability Analysis of the Long-term Storage of Carbon Dioxide in Deep Saline Aquifers, Adv. Water Resources, pp. 397–407, 29, 2006.
[33] Xie, Y., Simmons, C.T. & Werner, A.D., Speed of Free Convective Fingering in Porous Media, Water Resour. Res., W11501, 47, 2011.